

Variable optical chirality in atomic assisted microcavity

Hao Zhang(张浩), Wen-Xiu Li (李文秀), Peng Han(韩鹏), Xiao-Yang Chang(常晓阳), Shuo Jiang(蒋硕), An-Ping Huang(黄安平), Zhi-Song Xiao(肖志松)

Citation: Chin. Phys. B . 2020, 29(11): 114207 . **doi:** 10.1088/1674-1056/abb660
Journal homepage: http://cpb.iphy.ac.cn; http://iopscience.iop.org/cpb

What follows is a list of articles you may be interested in

Microwave frequency transfer over a 112-km urban fiber link based on electronic phase compensation

Wen-Xiang Xue(薛文祥), Wen-Yu Zhao(赵文宇), Hong-Lei Quan(全洪雷), Cui-Chen Zhao(赵粹臣), Yan Xing(邢燕), Hai-Feng Jiang(姜海峰), Shou-Gang Zhang(张首刚)

Chin. Phys. B . 2020, 29(6): 064209 . **doi:** 10.1088/1674-1056/ab84d6

Square microcavity semiconductor lasers

Yuede Yang(杨跃德), Haizhong Weng(翁海中), Youzeng Hao(郝友增), Jinlong Xiao(肖金龙), Yongzhen Huang(黄永箴)

Chin. Phys. B . 2018, 27(11): 114212 . **doi:** 10.1088/1674-1056/27/11/114212

Electrically pumped metallic and plasmonic nanolasers

Martin T Hill

Chin. Phys. B . 2018, 27(11): 114210 . **doi:** 10.1088/1674-1056/27/11/114210

Theoretical analysis of the electromagnetic field inside an anomalous-dispersion microresonator under synthetical pump

Xin Xu(徐昕), Xiaohong Hu(胡晓鸿), Ye Feng(冯野), Yuanshan Liu(刘元山), Wei Zhang(张伟), Zhi Yang(杨直), Wei Zhao(赵卫), Yishan Wang(王屹山)

Chin. Phys. B . 2016, 25(3): 034208 . **doi:** 10.1088/1674-1056/25/3/034208

Sub-Poissonian photon emission in coupled double quantum dots–cavity system

Ye Han, Peng Yi-Wei, Yu Zhong-Yuan, Zhang Wen, Liu Yu-Min

Chin. Phys. B . 2015, 24(11): 114202 . **doi:** 10.1088/1674-1056/24/11/114202

Variable optical chirality in atomic assisted microcavity*

Hao Zhang(张浩)[2], Wen-Xiu Li (李文秀)[1], Peng Han(韩鹏)[1], Xiao-Yang Chang(常晓阳)[1], Shuo Jiang(蒋硕)[1], An-Ping Huang(黄安平)[1], and Zhi-Song Xiao(肖志松)[1,3,†]

[1] *Key Laboratory of Micro-nano Measurement, Manipulation and Physics (Ministry of Education), School of Physics, Beihang University, Beijing* 100191, *China*

[2] *Research Institute of Frontier Science, Beihang University, Beijing* 100191, *China*

[3] *Beijing Academy of Quantum Information Sciences, Beijing* 100193, *China*

(Received 17 May 2020; revised manuscript received 31 August 2020; accepted manuscript online 9 September 2020)

The manipulating of optical waves in a microcavity is essential to developing the integrated optical devices. Generally, the two eigenmodes in a whispering-gallery-mode (WGM) microcavity possess chiral symmetry. Here we show the chiral symmetry breaking is induced by the asymmetric backscattering of counter-propagating optical waves in a whispering-gallery-mode (WGM) microcavity with a cavity-made slot filled with atomic vapor. Through tuning the dispersion relation of the atomic vapor in the cavity-made slot, the chiral modes are continuously steered. The mode frequency splitting in the transmission and reflection spectra stem from the chiral symmetry breaking of the two eigenmodes. The displacement sensitivity of the proposed system in response to the length variation of cavity-made slot exhibits a high sensitivity value of 15.22 THz/nm.

Keywords: microcavity, optical chirality, dispersion

PACS: 42.60.Da, 42.50.–p, 42.79.Gn, 42.81.Pa **DOI:** 10.1088/1674-1056/abb660

1. Introduction

Optical microcavity with high-Q factor and small mode volume can significantly enhance light–matter interactions, and plays an ideal platform for realizing micro/nano-scale integrated optical components including sensors, modulators, and lasers. Generally, the two travelling wave modes, *i.e.*, clockwise (CW) and counterclockwise (CCW), are sustained in an optical microcavity with the geometry symmetry. The mirror reflection symmetry of a microcavity can be broken by the cross-coupling between CW and CCW waves induced by a perturbation on the periphery of the microcavity. For example, a particle on the edge of a whispering-gallery-mode (WGM) microcavity leads to the cross-coupling between CW and CCW waves due to the backscattering, and the two standing wave modes with equal weights are generated.[1] Because of the mirror reflection geometry symmetry, the microcavity with a pair of standing wave modes possesses chiral symmetry, exhibiting that the transmission or reflection spectra are identical at the two ports of the input–output taper fiber nearby the WGM microcavity. The manipulating of optical waves to break the chiral symmetry in a microcavity is vital to both the research of microcavity photonics and the development of integrated optical devices such as unidirectional lasers,[2–4] highly sensitive sensors,[5,6] and all-optical memories.[7,8]

Chiral symmetry breaking is derived from breaking either parity[1,3,9,10] or time-reversal symmetry.[11–13] For the parity symmetry breaking, deformed microdisks are first utilized to realize the chiral behaviour and directional light emission.[9,10] In an open quantum system, the asymmetric backscattering of the propagating optical fields induced by the nanoparticles adhering to the surface of the microcavity has been demonstrated.[1] A strong chiral behaviour with unbalanced contributions of the backscattering is shown in the microcavity. For controlling the flow of light and laser emission, Peng *et al.* used two nano-tips as Rayleigh scatterers to steer optical modes at an exceptional point (EP).[3] An open system described by Non-Hermitian Hamiltonian exhibits many intriguing physical phenomena at a singularity, called EP, at which the eigenvalues and the corresponding eigenvectors coalesce.[4–16] Chirality is a fascinating asymmetric phenomenon in the vicinity of the EP, where the cavity retains only one mode (CW or CCW) and exhibits the maximum chirality value 1 or -1.[3,17] On the other hand, chiral symmetry breaking in an optical microcavity will also appear when the time-reversal symmetry is broken such as rotation.[11–13]

In this paper, we demonstrate that the chiral modes are manipulated via a cavity-made slot filled with atomic vapor in a WGM microcavity. We also analyze the displacement sensitivity of our system in response to the length variation of cavity-made slot for the sensing applications.

*Project supported by the National Natural Science Foundation of China (Grant Nos. 11574021, 61975005, and 11804017) and the Fund from Beijing Academy of Quantum Information Sciences, China (Grant No. Y18G28).

†Corresponding author. E-mail: zsxiao@buaa.edu.cn

© 2020 Chinese Physical Society and IOP Publishing Ltd

2. Theoretical mode and analysis

Two eigenmodes in a microcavity are excited by an evanescent field with a coupling rate κ_{ex} rooted from an input–output bus waveguide as depicted in Fig. 1. A cavity-made slot filled with atomic vapor is perpendicular to the light propagating direction on the edge of the toroidal microcavity. Due to the reflection of this slot, there is a cross-coupling rate $\gamma_{c1,2}$ between CW and CCW propagating WGM, where the CW (CCW) mode represented by 1 (2) is coupled into CCW (CW) mode.

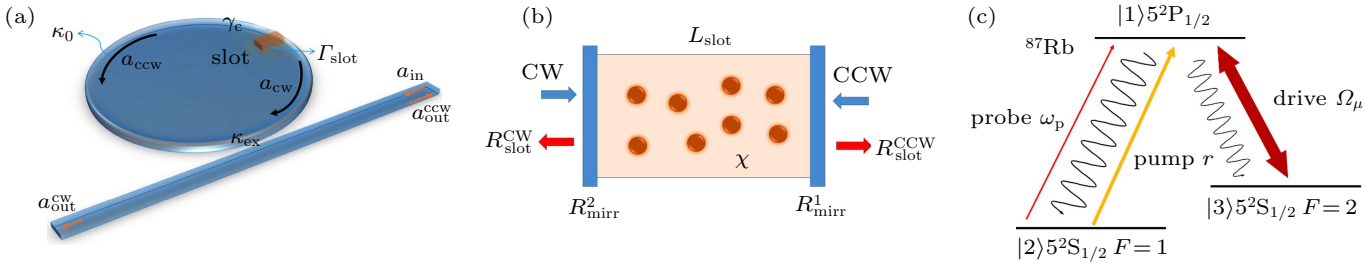


Fig. 1. (a) Schematic diagram of WGM microcavity coupled with (b) cavity-made slot and (c) filled with three-level atomic vapor.

2.1. Cavity-made slot with three-level atomic system

The cavity-made slot is filled with a three-level Rb atomic vapor and develops into a dispersive cavity when we manipulate the dispersive relation of atoms by optical pump and driving field. Through adjusting the optical pump rate r acting on energy levels $|1\rangle \to |2\rangle$ and strong driving field Rabi frequency Ω_μ acting on $|1\rangle \to |3\rangle$, it will lead the probe light in the slot to undergo normal or anomalous dispersion.[18] The cavity-made slot with normal dispersion displays a narrower resonance linewidth than an empty slot cavity without atomic vapor. Hence, the effective reflectivity $R_{slot}^{CCW,CW}$ of the cavity-made slot will be changed more to the resonance frequency in the condition of normal dispersion. The effective reflectivity of the cavity-made slot is

$$R_{slot}^{ccw,cw} = \left| r_{mirr}^{1,2} + \frac{(1-R_{mirr}^{1,2}) r_{mirr}^{2,1} a_{slot} \cdot e^{2i(d\omega_{12}/c)[1-(\Delta/\omega_{12})]n_{slot}(\Delta)}}{1 - r_{mirr}^{1} r_{mirr}^{2} a_{slot} \cdot e^{2i(d\omega_{12}/c)[1-(\Delta/\omega_{12})]n_{slot}(\Delta)}} \right|^2, \tag{1}$$

where α_{slot} is the loss coefficient and $a_{slot} = \exp(-\alpha_{slot} d/2)$ is the propagation amplitude attenuation. The refractive index n_{slot} is related to the susceptibility $n_{slot} \approx 1 + \chi/2$. The declarations of variables see Table 1. When the surface reflectivities of the cavity-made slot satisfy $R_{mirr}^{1} = R_{mirr}^{2}$, the effective reflectivities R_{slot}^{CCW} and R_{slot}^{CW} are identical for the both CW and CCW waves in the microresonantor, and now this is a reciprocal structure. Once the surface reflectivities $R_{mirr}^{1} \neq R_{mirr}^{2}$, the reciprocity of the microresonator is broken. Thus, the cavity-made slot can be seen as an optical isolator, the isolation ratio (IR) of this structure is given by

$$\mathrm{IR} = 10 \times \log_{10}\left(\frac{R_{slot}^{cw}}{R_{slot}^{ccw}}\right). \tag{2}$$

In order to exhibit a larger value of IR, we set a surface reflectivity of the slot R_{mirr}^{2} to be a high value of 0.999. Scaning the other surface reflectivity R_{mirr}^{1} to achieve the maximal value of IR with different values of atomic pump rate r and driving field Rabi frequency Ω_μ.

In Fig. 2, the effective reflection rate of CW wave R_{slot}^{CCW} slowly declines from one due to the increase of R_{mirr}^{1} and intersects with R_{slot}^{CCW} when R_{mirr}^{1} is 0.999. There is always a minimal value approaching to zero for the effective reflection rate of CCW wave R_{slot}^{CCW}, and the corresponding value of R_{mirr}^{1} is close to one with the decrease of pump rate r or increase of driving field Ω_μ. Thus, it can be deduced that the maximal isolation ratio IR_{max} will appear at this point.

Table 1. Simulation parameters.

Symbols	Meaning
κ_{ex}	external coupling between microresonator and waveguide
κ_0	intrinsic loss in the microresonator
$\gamma_{c1,2}$	cross-coupling rate between CW and CCW waves
r	pump rate acting on energy levels $\|1\rangle \to \|2\rangle$
Ω_μ	driving field Rabi frequency acting on $\|1\rangle \to \|3\rangle$
γ	decay rate from state $\|1\rangle \to \|2\rangle$
$R_{slot}^{CW,CCW}$	effective reflectivity of cavity-made slot
$R_{mirr}^{1,2}$	reflectivity of slot surface
R_0	radius of microresonator
α_{slot}	field propagation loss into atomic vapor
a_{slot}	propagation amplitude attenuation when light travels through slot
n_0	refractive index of microresonator
χ	susceptibility of atomic vapor
ω_{12}	transition frequency from $\|2\rangle \to \|1\rangle$
ω_p	frequency of probe field
γ_{total}	total loss rate for microresonator
Γ_{slot}	absorption loss rate of atomic vapor
τ_0	optical round-trip time in microresonator

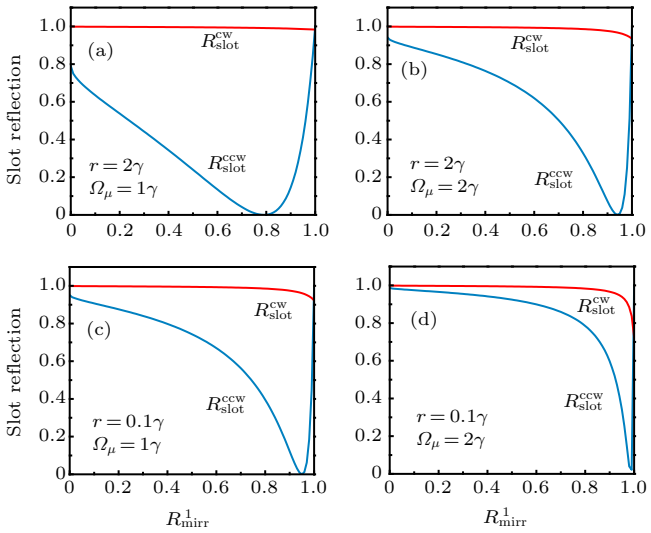


Fig. 2. The slot reflection to the CCW and CW waves varying with the slot surface reflection $R^1_{\rm mirr}$ at panel (a) $r = 2\gamma$ and $\Omega_\mu = \gamma$, panel (b) $r = 2\gamma$ and $\Omega_\mu = 2\gamma$, panel (c) $r = 0.1\gamma$ and $\Omega_\mu = 1\gamma$, and panel (d) $r = 0.1\gamma$ and $\Omega_\mu = 2\gamma$. The length of the cavity-made slot is set to be $L_{\rm slot} = 6c\pi/\omega_{12}$ which is 3 wavelengths at ω_{12}.

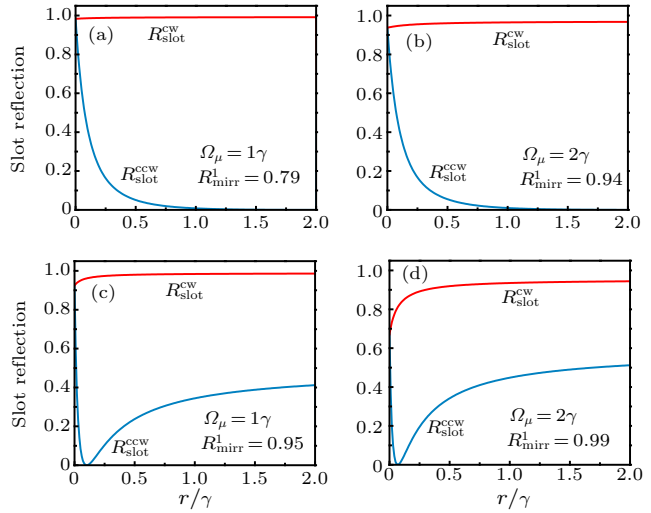


Fig. 3. The slot reflection to the CCW and CW waves varying with the pump rate r at panel (a) $\Omega_\mu = \gamma$ and $R^1_{\rm mirr} = 0.79$, panel (b) $\Omega_\mu = 2\gamma$ ad $R^1_{\rm mirr} = 0.94$, panel (c) $\Omega_\mu = 1\gamma$ and $R^1_{\rm mirr} = 0.95$, and panel (d) $\Omega_\mu = 2\gamma$ and $R^1_{\rm mirr} = 0.99$.

According to the values of $R^1_{\rm mirr}$ corresponding to the maximal $\rm IR_{max}$ in Figs. 2(a)–2(d), we plot the variations of effective reflection of counter-propagating waves on the cavity-made slot in the microresonator with pump rate at different driving field Rabi frequencies: $\Omega_\mu = \gamma$ or $\Omega_\mu = 2\gamma$ in Figs. 3(a)–3(d). With the increase of pump rate in Figs. 3(a)–3(d), the values of effective reflection rate $R^{\rm CW}_{\rm slot}$ are raised slowly, while the values of effective reflection rate $R^{\rm CCW}_{\rm slot}$ significantly decline to nearly zero and increase slightly to reach a steady value.

Next, in Fig. 4 the curves for IR of the cavity-made slot versus pump rate r are plotted at the different optimum values of $R^1_{\rm mirr}$ obtained in Fig. 2. The maximal value of isolation ratio $\rm IR_{max}$ can be obtained to be as high as 113 dB at $R^1_{\rm mirr} = 0.79$ and $\Omega_\mu = \gamma$.

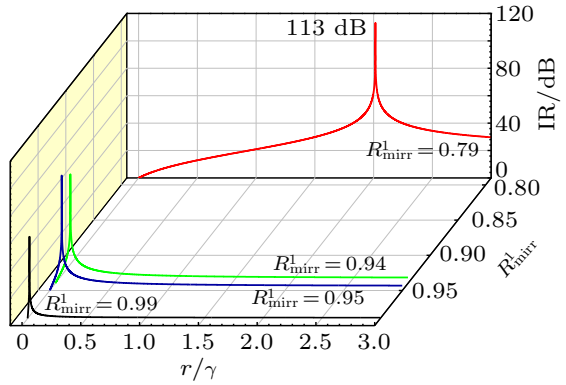


Fig. 4. The IR values adjusted by controlling pump rate r at four optimum values of $R^1_{\rm mirr}$ obtained in Fig. 2 when the driving field Rabi frequency is $\Omega_\mu = \gamma$.

2.2. Cavity-made slot WGM mircoresonator

As shown in Fig. 1, due to the reflection of the CW and CCW waves on cavity-made slot in the resonator, the cross-coupling between CW and CCW occurs. A pair of degenerate modes supported in WGM resonator are turned into non-degenerate WGMs, exhibiting mode broadening or splitting in transmission spectrum and reflection spectrum. In a WGM resonator, the asymmetric backscattering of counter-propagating optical wave on the cavity-made slot can be related to chiral behaviour, such as in the process of achieving maximal chirality and unidirectional emission. Hence, the chirality behaviour in the slot microresonator we proposed can be controlled by the reflection characteristic of the cavity-made slot. To be specific, through adjusting the pump rate and driving field acting on atomic vapor into the cavity-made slot, the susceptibility of the atomic vapor can be artificially constructed to control the reflection of the cavity-made slot.

The coupled mode equations of the propagating CW and CCW modes are

$$\begin{aligned}\dot{a}_{\rm cw} &= -[{\rm i}\Delta\omega + {\rm i}\gamma_{\rm c1} + \gamma_{\rm total}]a_{\rm cw} \\ &\quad - \left[{\rm i}\gamma_{\rm c1} + \frac{\Gamma_{\rm slot}}{2}\right]a_{\rm ccw} - \sqrt{\kappa_{\rm ex}}a_{\rm in}, \qquad (3)\\ \dot{a}_{\rm ccw} &= -[{\rm i}\Delta\omega + {\rm i}\gamma_{\rm c2} + \gamma_{\rm total}]a_{\rm ccw} \\ &\quad - \left[{\rm i}\gamma_{\rm c2} + \frac{\Gamma_{\rm slot}}{2}\right]a_{\rm cw}, \qquad (4)\end{aligned}$$

where $\Delta\omega = \omega - \omega_{\rm c}$ is the optical frequency detuning from the microresonator's resonant angular frequency $\omega_{\rm c}$. The total loss rate is $\gamma_{\rm total} = (\Gamma_{\rm slot} + \kappa_0 + \kappa_{\rm ex})/2$, where $\Gamma_{\rm slot}$ is the absorption loss rate derived from atom vapor into the cavity-made slot.

According to the input–output relation of microresonator and bus waveguide, the output transmission and reflection spectra from the bus waveguide are

$$T=\left|\frac{a_{\rm cw}^{\rm out}}{a_{\rm in}}\right|^2=\left|1+\frac{\kappa_{\rm ex}(\mathrm{i}\Delta\omega+\mathrm{i}\gamma_{\rm c2}+\gamma_{\rm total})}{(\mathrm{i}\gamma_{\rm c1}+\Gamma_{\rm slot}/2)(\mathrm{i}\gamma_{\rm c2}+\Gamma_{\rm slot}/2)-(\mathrm{i}\Delta\omega+\mathrm{i}\gamma_{\rm c1}+\gamma_{\rm total})(\mathrm{i}\Delta\omega+\mathrm{i}\gamma_{\rm c2}+\gamma_{\rm total})}\right|^2,$$
$$R=\left|\frac{a_{\rm ccw}^{\rm out}}{a_{\rm in}}\right|^2=\left|\frac{-\kappa_{\rm ex}(\mathrm{i}\gamma_{\rm c2}+\Gamma_{\rm slot}/2)}{(\mathrm{i}\gamma_{\rm c1}+\Gamma_{\rm slot}/2)(\mathrm{i}\gamma_{\rm c2}+\Gamma_{\rm slot}/2)-(\mathrm{i}\Delta\omega+\mathrm{i}\gamma_{\rm c1}+\gamma_{\rm total})(\mathrm{i}\Delta\omega+\mathrm{i}\gamma_{\rm c2}+\gamma_{\rm total})}\right|^2. \quad (5)$$

The cross-coupling rate $\gamma_{\rm c1,2}$ between CW and CCW waves is

$$\gamma_{\rm c1,2}=\left|R_{\rm slot}^{\rm ccw,cw}\right|/\tau_0-\gamma_{\rm total}, \quad (6)$$

where $\tau_0=2\pi n_{\rm ring}R_0/c$ is the optical round-trip time in the resonator with a radius R_0. When the $\gamma_{\rm c1,2}<0$, the counterclockwise mode $a_{\rm ccw}$ will be depleted due to the total loss rate $\gamma_{\rm total}$ in the WGM resonator and cannot be reflected by the other side of the cavity-made slot. Therefore, neither of the clockwise mode $a_{\rm cw}$ and counterclockwise mode $a_{\rm ccw}$ can exist simultaneously. The effective reflectivity $R_{\rm slot}^{\rm CCW,CW}$ should be large enough or the total loss rate $\gamma_{\rm total}$ should be reduced to ensure the $\gamma_{\rm c1,2}$ is positive, and the two modes can both exist in the cavity simultaneously. Due to cross-coupling rate $\gamma_{\rm c1,2}$ two new eigenmodes with eigenfrequencies are

$$\omega_\pm=\Delta\omega+\left(\frac{\gamma_{\rm c1}+\gamma_{\rm c2}}{2}\right)-\mathrm{i}\gamma_{\rm total}\pm\sqrt{\frac{1}{4}(\gamma_{\rm c1}-\gamma_{\rm c2})^2+(\gamma_{\rm c1}-\mathrm{i}\Gamma_{\rm slot}/2)(\gamma_{\rm c2}-\mathrm{i}\Gamma_{\rm slot}/2)}. \quad (7)$$

3. Tuning chiral modes

The cavity-made slot is seen as a tunable reflector and generates two standing wave modes in the mircoresonator, symmetric mode (SM) and asymmetric mode (ASM),[19] which are manifested by the doublet in the transmission and reflection spectra in Fig. 5. The SM experiences a significant frequency redshift, and the ASM has no shift. The curves of transmission and reflection versus $\Delta\omega$ for four different value of pump rate r, *i.e.*, 0.1γ, 0.2γ. 0.3γ, and 0.4γ are shown in Fig. 5(a), and those for four different values of driving field frequency Ω_μ, *i.e.*, 7γ, 8γ, 9γ and 10γ are displayed in Fig. 5(b). With the increase of pump rate r, the frequency splitting between SM and ASM decreases in Fig. 5(a) and the ASM modes are broadened (see the inset of Fig. 5(a)), resulting from the weakness of cross-coupling between CW and CCW waves. Narrow resonance linewidth of the cavity-made slot induced by normal dispersion is sensitive to the reflection response and enhances the cross-coupling between CW and CCW waves in the microresonator.[20] In Fig. 5(b), the frequency splitting increases with driving field frequency Ω_μ increasing, the linewidth of SM and ASM modes are narrowed due to the enhancement of normal dispersion of atomic vapor into the cavity-made slot.

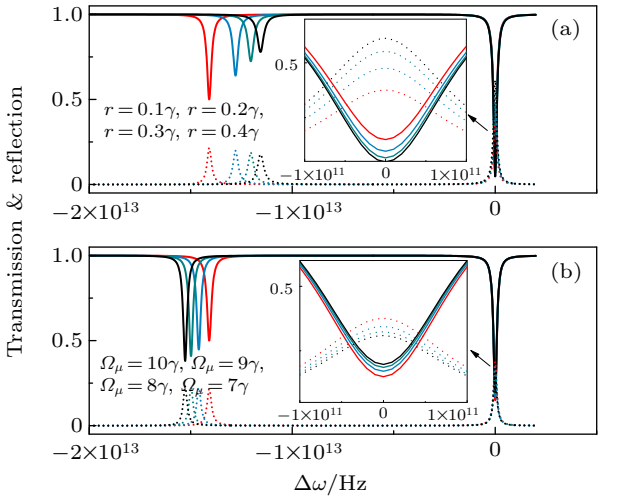


Fig. 5. (a) Transmission and reflection spectra *versus* $\Delta\omega$ for four values of pump rate r (0.1γ, 0.2γ, 0.3γ, and 0.4γ) and driving field frequency $\Omega_\mu=7\gamma$. (b) Transmission and reflection spectra *versus* $\Delta\omega$ for four values of driving field frequency Ω_μ (7γ, 8γ, 9γ, and 10γ) and $r=0.1\gamma$. [(a) and (b)] Insets show magnified details of no shifted peaks of transmission and reflection spectra.

The chirality $\alpha_{\rm TR}$ of a resonator is defined as follows:

$$\alpha_{\rm TR}=\frac{||T|-|R||}{|T|+|R|}. \quad (8)$$

In order to ensure the existence of the cross-coupling rate $\gamma_{\rm c1,2}$ between CW and CCW waves in the microresonator, we use the value of driving field frequency $\Omega_\mu=7\gamma$ with $R_{\rm mirr}^1=0.99$ in Fig. 5. The slot IR denoting asymmetric backscattering on each of sides of the cavity-made slot is shown in Fig. 6(a). The normal dispersion condition is represented by the green shaded area. The curves of chirality $\alpha_{\rm TR}$ *versus* r/γ for different driving field frequencies are plotted in Fig. 6(b), and the maximum chirality approaches to 1. The asymmetric backscatterings on both sides of the cavity-made slot bring about the asymmetric cross-coupling between CW and CCW waves. Through steering the pump rate r acting on atomic vapor, the chirality induced by the asymmetric cross-coupling between CW and CCW waves is continuously tuned. The chirality with the value $\Omega_\mu=7\gamma$ represented by the black curve has an evident elevation with the increase of pump rate r in the normal dispersion condition ($r<\gamma$) and reaches a steady state value with a maximum chirality of 0.999 in the anomalous dispersion condition ($r>\gamma$) as indicated in Fig. 6. The variation range of the chiral behavior decreases when the driving field strengthens.

It is necessary to introduce the frequency splitting quality factor $Q_{\rm sp}$ to evaluate the experimental observability of the real

frequency splitting.[21] The frequency splitting quality factor $Q_{\rm sp}$ is defined as

$$Q_{\rm sp} = \frac{|{\rm Re}(\omega_+) - {\rm Re}(\omega_-)|}{-{\rm Im}(\omega_+) - {\rm Im}(\omega_-)}. \tag{9}$$

The $Q_{\rm sp}$ is plotted in Fig. 6(c) and decreases with the increase of pump rate r since the asymmetric backscatterings are enhanced under the normal dispersion condition of the atomic vapor. On the other hand, the larger the driving field frequency, the smaller the adjustable range of $Q_{\rm sp}$ is. In the normal dispersion region in the shaded area of Fig. 6, the chirality and $Q_{\rm sp}$ prominently vary with the increase of pump rate. In Fig. 6, it is also confirmed that as the chiralityincreases, the frequency splitting quality $Q_{\rm sp}$ decreases. Moreover, in a passive system it is difficult to observeexperimentally if the frequency splitting quality $Q_{\rm sp} < 1$.[9] It needs to introduce the gain into system, such as doping Er^{3+} in the WGM microcavity, to narrow the resonance linewidth for overcoming this experimental difficulty. However, in our slot microresonator system the $Q_{\rm sp}$ is larger than 25 as shown in Fig. 6(c), it not only avoids introducing gain into the system, but also has a distinct frequency splitting.

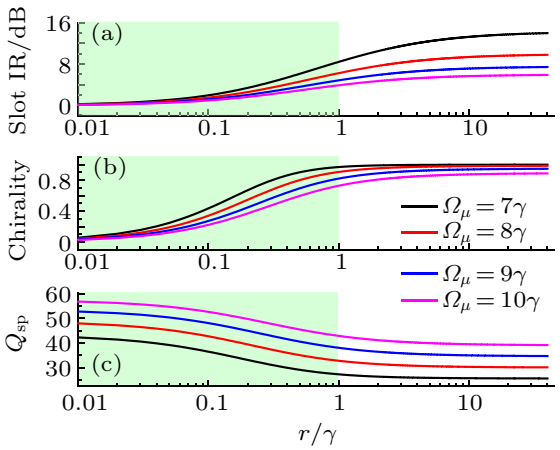


Fig. 6. (a) Slot IR representing asymmetric backscattering of cavity-made slot, (b) chirality continuously tuned via steering pump rate r, (c) frequency splitting quality $Q_{\rm sp}$ *versus* pump rate, with shaded regions representing normal dispersion, and blank regions referring to anomalous dispersion. Some parameters used here are as follows: $\kappa_0 = \kappa_{\rm ex} = 1 \times 10^{11}$ Hz, $R^1_{\rm mirr} = 0.99$, $R^2_{\rm mirr} = 0.999$, radius of WGM microcavity $R_0 = 30\lambda/(2\pi n_0)$, and refractive index $n_0 = 1.5$.

Next, we consider the length variation of the cavity-made slot in our system in response to a measurable perturbation for displacement sensing applications, such as cavity optomechanical mode or pressure induced expansion of the cavity. Here, to avoid redundancy, we mainly discuss the frequency splitting in the transmission spectrum induced by the change of the length of cavity-made slot. The mode degeneracy of WGM microcavity is lifted due to the cavity-made slot, which creates two standing wave modes (SM and ASM) discussed in the above section. The SM is mainly affected by the change of slot length, while it has almost no influence on ASM.

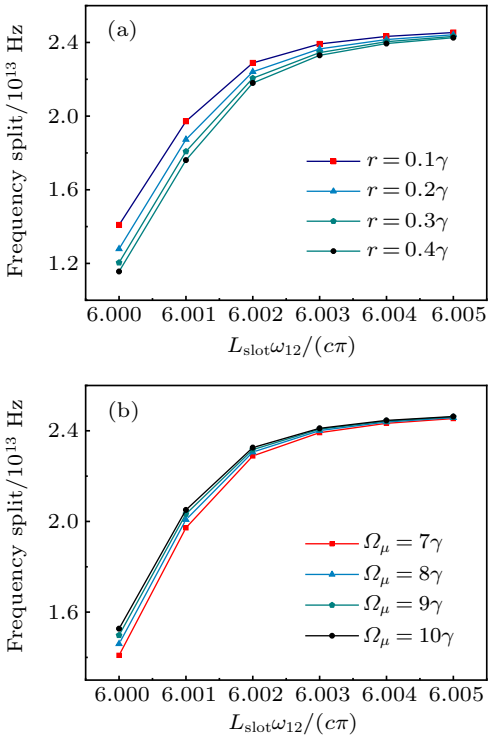


Fig. 7. Curves of frequency split *versus* $L_{\rm slot}\omega_{\rm p}$ in transmission with (a) driving field frequency $\Omega_\mu = 7\gamma$ for $r = 0.1\gamma$, 0.2γ, 0.3γ, and 0.4γ, and (b) pump rate $r = 0.4\gamma$ for $\Omega_\mu = 7\gamma$, 8γ, 9γ, and 10γ.

The modes splittings of transmission spectrum, induced by the variation of the length of slot $L_{\rm slot}$, are shown in Fig. 7 with different values of pump rate r in Fig. 7(a) and different values of diving field frequency Ω_μ in Fig. 7(b). Figures 7(a) and 7(b) show that the increases of frequency splittings gradually decrease with the length of slot $L_{\rm slot}$ increasing. The frequency splitting increases with pump rate r decreasing in Fig. 7(a) due to the enhancement of normal dispersion of the atomic vapor into the slot. In Fig. 7(b), the frequency splitting decreases with driving field frequency Ω_μ increasing due to the weakening of the normal dispersion of the vapor. According to Fig. 7(b), the maximum splitting response is 15.22 THz/nm at $\Omega_\mu = 7$ and $r = 0.4\gamma$. Hence, an equivalent length resolution can be estimated by the linewidth of the transmission spectrum in Fig. 5. The linewidth of SM at $\Omega_\mu = 7$ and $r = 0.4\gamma$ is 0.465 THz, thus, the equivalent length resolution is

$$\Delta L_{\rm min} = \frac{\Delta\omega_{\rm FWHM}}{15.22\ {\rm THz/nm}} \approx 3 \times 10^{-11}\ {\rm m}. \tag{10}$$

Finally, the future experimental realization of the proposal will be discussed primarily. The Q-factor of microresonator can be calculated by $Q = \omega_{\rm p}/2\gamma_{\rm total} \approx 8.3 \times 10^3$ through the simulation parameters in this paper. In addition, the vapor slot may be more easily implemented in experiment on fiber. And we find that the nanofiber with several-hundred nanometer in diameter can be surrounded by atoms, and the evanescent field of the propagating mode in the nanofiber can interact with the atoms.[22,23]

4. Conclusions and perspectives

In this work, the chiral symmetry breaking in a WGM microcavity with a cavity-made slot filled with atomic vapor is present. A pair of tunable chiral modes are engineered via controlling pump rate acting on atomic vapor to change dispersion relation in the cavity-made slot. The maximum isolation ratio between CW and CCW waves is approximately 113 dB. To evaluate the experimental observability of the real frequency splitting in our system, the frequency splitting quality $Q_{\rm sp} > 25$, it does not need to introduce gain into our system for observing a conspicuous frequency splitting. The system exhibits a high displacement sensitivity value of 15.22 THz/nm in response to the variation of the length of cavity-made slot, and the equivalent length resolution is 3×10^{-11} m. Operating chiral modes in WGM microcavities has important implications to realize the high-performance on-chip sensors.

References

[1] Wiersig J 2014 *Phys. Rev. Lett.* **112** 203901
[2] Redding B, Ge L, Song Q H, Wiersig J, Solomon G S and Cao H 2012 *Phys. Rev. Lett.* **108** 253902
[3] Peng B, Ozdemir S K, Liertzer M, Chen W J, Kramer J, Yilmaz H, Wiersig J, Rotter S and Yang L 2016 *Proc. Nat. Acad. Sci. USA* **113** 6845
[4] Wang W H, Liu S, Gu Z Y and Wang Y 2020 *Phys. Rev. A* **101** 013833
[5] Baaske M D, Foreman M R and Vollmer F 2014 *Nat. Nanotechnol.* **9** 933
[6] Shen B Q, Yu X C, Zhi Y Y, Wang L, Kim D H, Gong Q H and Xiao Y F 2016 *Phys. Rev. Appl.* **5** 024011
[7] Hill M T, Dorren H J S, de Vries T, Leijtens X J M, den Besten J H, Smalbrugge B, Oei Y S, Binsma H, Khoe G D and Smit M K 2004 *Nature* **432** 206
[8] Liu L, Kumar R, Huybrechts K, Spuesens T, Roelkens G, Geluk E J, de Vries T, Regreny P, Van Thourhout D, Baets R and Morthier G 2010 *Nat. Photon.* **4** 182
[9] Wiersig J and Hentschel M 2008 *Phys. Rev Lett.* **100** 033901
[10] Wiersig J, Eberspacher A, Shim J B, Ryu J W, Shinohara S, Hentschel M and Schomerus H 2011 *Phys Rev. A* **84** 023845
[11] Shu F J, Zou C L, Zou X B and Yang L 2016 *Phys. Rev. A* **94** 013848
[12] Ge L, Sarma R and Cao H 2015 *Optica* **2** 323
[13] Sarma R, Ge L, Wiersig J and Cao H 2015 *Phys. Rev. Lett.* **114** 053903
[14] Chen W J, Ozdemir S K, Zhao G M, Wiersig J and Yang L 2017 *Nature* **548** 192
[15] Hodaei H, Hassan A U, Wittek S, Garcia-Gracia H, El-Ganainy R, Christodoulides D N and Khajavikhan M 2017 *Nature* **548** 187
[16] Kullig J and Wiersig J 2019 *Phys. Rev. A* **100** 043837
[17] Wang C Q, Jiang X F, Zhao G M, Zhang M Z, Hsu C W, Peng B, Stone A D, Jiang L and Yang L 2020 *Nat. Phys.* **16** 334
[18] Xu J P, Al-Amri M, Yang Y P, Zhu S Y and Zubairy M S 2012 *Phys. Rev. A* **86** 033828
[19] Zhu J G, Ozdemir S K, Xiao Y F, Li L, He L N, Chen D R and Yang L 2010 *Nat. Photon.* **4** 122
[20] Zhang H, Li W X, Han P, Chang X Y, Liu J M, Huang A P and Xiao Z S 2019 *J. Appl. Phys.* **125** 084502
[21] Wiersig J 2016 *Phys. Rev. A* **93** 033809
[22] Liu R J, Su D Q, Song Z X, Ji Z H and Zhao Y T 2019 *Chin. Phys. B* **28** 124201
[23] Song Z X, Yue X Y, Luo Y, Li H D and Zhao Y T 2019 *Chin. Opt. Lett.* **17** 031901